

Journal of Materials Chemistry A

Accepted Manuscript



This is an *Accepted Manuscript*, which has been through the Royal Society of Chemistry peer review process and has been accepted for publication.

Accepted Manuscripts are published online shortly after acceptance, before technical editing, formatting and proof reading. Using this free service, authors can make their results available to the community, in citable form, before we publish the edited article. We will replace this *Accepted Manuscript* with the edited and formatted *Advance Article* as soon as it is available.

You can find more information about *Accepted Manuscripts* in the [Information for Authors](#).

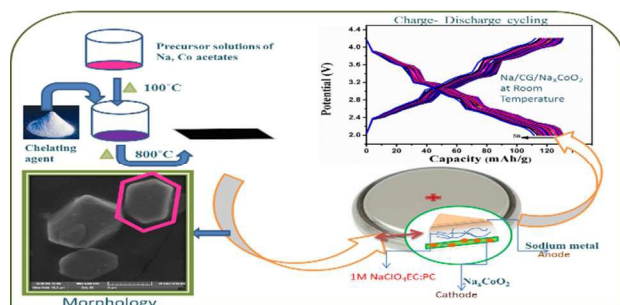
Please note that technical editing may introduce minor changes to the text and/or graphics, which may alter content. The journal's standard [Terms & Conditions](#) and the [Ethical guidelines](#) still apply. In no event shall the Royal Society of Chemistry be held responsible for any errors or omissions in this *Accepted Manuscript* or any consequences arising from the use of any information it contains.

Graphical Abstract

High Performing Na_xCoO_2 as a Cathode material for Rechargeable Sodium Batteries”

B Venkata Rami Reddy, R Ravikumar, C Nithya and S Gopukumar*

High performing Na_xCoO_2 cathode material for sodium ion battery synthesized using sol-gel combustion technique using glycine as a chelating agent.



High Performing Na_xCoO_2 as a Cathode material for Rechargeable Sodium Batteries

Cite this: DOI: 10.1039/x0xx00000x

B Venkata Rami Reddy^a, R Ravikumar^a, C Nithya^b and S Gopukumar^{*a}

Received 00th January 2012,
Accepted 00th January 2012

DOI: 10.1039/x0xx00000x

www.rsc.org/

Sodium cobalt oxide (NCO) has been synthesized by glycine assisted sol-gel combustion method. XRD studies confirms the P2 phase formation of NCO. Na exists in two different environment in NCO crystallite structure, which is confirmed by ^{23}Na Nuclear Magnetic Resonance spectra (NMR). Morphological studies confirms that the particles are unique with stacked hexagonal shape. Galvanostatic charge/discharge studies performed at different current rates (0.1, 0.2 and 0.5) delivers the reversible specific capacities of 126, 108 and 77 mAhg^{-1} respectively. Further, life cycle performance after 50 cycles exhibit at 0.1C rate, delivers an average discharge capacity of $\sim 121 \text{mAh g}^{-1}$ with capacity retention of $\sim 86\%$ (Coulombic efficiency $\sim 99.9\%$). The investigated NCO's superior performance suggests the suitability as a cathode material for Na-ion batteries.

Introduction

Since 1990s, Li-ion batteries (LIBs) are playing a vital role in portable electronic devices such as mobiles, laptops, tablets and electric vehicles etc., owing to its compact size and high energy density.^{1,2} In view of the high cost and less abundance of lithium, the whole world is looking for an alternative material to meet the future energy demands. Unlike lithium, sodium is widely existing and the most abundant element all over the world. In order to make a cost effective battery, at present researchers are focussing towards Na-ion batteries (NIB).³⁻⁶ Since, the redox potential of sodium is closer to lithium, researchers are glued towards sodium ion battery chemistry which could be amicable for LIB's. Reports on the class of cathode materials viz., phosphates⁷⁻⁹, perovskites¹⁰⁻¹³, NASICON^{12,13}, fluoro-sulphates, fluorophosphates^{14,15}, cyanides¹⁶ and oxides¹⁷⁻²¹ are available. Phosphate based materials, has been used as cathodes for Na-ion battery, but these materials possess maricite phase, which is thermally stable while on the other hand electrochemically inactive. Nazar *et al.*, synthesized metastable olivine materials like $\text{NaMnM}_{1-x}\text{PO}_4$ ($M=\text{Fe}, \text{Co}$), and exhibiting electrochemically interesting properties. Furthermore, the sodium ion extraction (partial) is a challenging task during cycling. Barpanda *et al.*,

prepared phosphate materials, which possess high potential window but delivers lesser capacity. Perovskite based materials like NaMF_3 ($M=\text{Mn}, \text{Fe}, \text{Co}, \text{Ni}$) also as cathodes for NIB, exhibiting better capacity at initial cycles, while on the other hand, handling as well as high polarisation effects are the major drawbacks for these kind of materials. NASICON type materials like $\text{Na}_3\text{V}_2\text{PO}_4$ has been extensively used as a cathode for NIB but the challenge is the low working potential (3.8 V) and poor conductivity. At present researchers are focusing on $(\text{FPO}_4)^{3-}$, $(\text{FSO}_4)^{3-}$ type cathode materials for sodium battery applications, but to improve conductivity and reduce volume expansion during cycling need to be overcome. Moreover, the above mentioned materials possess less theoretical capacity than the conventional oxide based cathodes. Till now, a few reports are published on metal oxide based cathodes.²²⁻²⁷ In the present investigation, we focussed on NCO, which is used as a cathode material for NIB. Generally, NCO has been synthesized by using various methods viz., solid state method, hydrothermal followed by solid state method, etc. Our earlier report²⁸ deals with the synthesis of NCO using inverse micro-emulsion method and evaluating the electrochemical behaviour. Herein, we present our investigation on NCO, synthesized via sol-gel combustion technique using glycine²⁹ as a chelating

agent as well as fuel which facilitates the uniform mixing, better yield and homogenous crystallite growth.

Experimental

NCO has been synthesized with sodium acetate (CH_3COONa) (Alfa Aesar) and Cobalt acetate ($\text{Co}(\text{CH}_3\text{COO})_2 \cdot 4\text{H}_2\text{O}$) (Alfa Aesar), Glycine (Merck). Stoichiometric amount of sodium acetate and cobalt acetates are dissolved in 20 ml of water so as to obtain 1 g of the product. However, an excess amount (20 %) of sodium acetate has been added to compensate for the sodium loss during calcination. The mixture was stirred for 1h at 70 °C and to this glycine (chelating agent) is being added (solution) drop by drop and followed by slow rise of temperature up to 100 °C so as to evaporate the water for obtaining transparent gel precursor. The gel was subjected to calcination at 800 °C for 6 hours. The crystallite properties of the annealed materials has been evaluated using an X-ray diffractometer (X'Pert PRO PANalytical PW 3040/60 X'Pert PRO) with $\text{Cu-K}\alpha$ radiation by measuring the diffraction angle (2θ) between 10 ° and 70 ° with an increment of 0.05 °/s. Solid ^{23}Na NMR spectra has been recorded for Na_xCoO_2 , using NMR instrument (BRUKER, 400MHz). FTIR spectrum for NCO has been run in between 400-2000 cm^{-1} (Model: Nicolex 5DX FTIR Spectrometer). Surface morphology of synthesized powder has been examined using a Field Emission Scanning Electron Microscope (FESEM Model: ZEISS). X-ray photoelectron spectroscopy of the synthesized powder was investigated using MULTILAB 2000 (Thermo scientific) photo electron spectrometer and the spectra recorded using an X-ray source ($\text{Mg-K}\alpha$ radiation 0-1253 eV). The electrochemical measurements have been carried out by fabricating 2032 type coin cells under argon-filled glove box with sodium metal as counter as well as reference electrode. The working electrode slurry is prepared by 80 % Na_xCoO_2 , 10% super-P carbon, and 10% PVDF (Polyvinylidene fluoride) binder blended with NMP (N-methyl-2-pyrrolidone) solvent and coated over an Al foil. The Polypropylene separator has been soaked in electrolyte and sandwiched between the electrodes. The galvanostatic charge-discharge studies has been carried out at different C-rates with the assembled coin cell using automatic battery cycle life tester (BaSyTECH MODEL) between 2.0 - 4.2 V. Cyclic voltammogram (CV) measurements were performed using an IVIUM STAT instrument with scan rates of 0.1, 1.0 and 5.0 mV s^{-1} between 2.0 - 4.2 V. The electrochemical impedance studies (EIS) have been carried out using FRA mode in AUTOLAB PGSTAT 204 with an AC signal of 5 mV in the frequency range from 100 KHz to 5 mHz.

Results and discussion

Fig. 1a depicts the TG/DTA of synthesized precursor in air atmosphere from ambient temperature to 1000 °C. In TGA curve two major weight loss regions have been observed between 80 and 150 °C and at the region 200 to 600 °C, further, beyond 600 °C here is no such major weight loss identified.

Weight loss occurring below 200 °C are due to the evaporation of superficial and absorbed water molecules. The major weight loss region between 200 and 600 °C (almost 50 %) is due to the decomposition of carbonates and glycine²⁹ which is supported with DTA curve with a strong exothermic peak observed at 550 °C. In DTA after 550 °C there is no such exothermic peak occurs. TG/DTA studies confirms that, phase formation will takes place a 600 °C. The XRD pattern of NCO has been recorded for the material heat treated at 800 °C for 6h in air, which shows formation of the phase pure NCO as shown in Fig.1b. The XRD patterns are indexed on the basis of hexagonal crystal system with P63/mmc space group and matches well with JCPDS file no. 00-087-0274. The peak parameters 'a, c' are 2.8202, 10.89 Å respectively and the cell volume is 75.07 Å³, are in confirmation with earlier reports.²⁵⁻²⁷ The XRD pattern for the electrode after cycling up to lower cut-off potential (2.0 V) has been illustrated in the Fig. S1. It infers that the most predominant broadened peaks for the same crystal structure has been retained, this is reflected in the FESEM images (Fig. S2) as well.

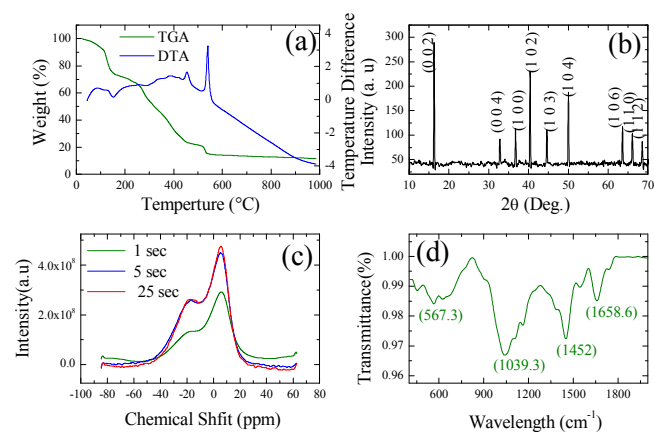


Fig.1. a) TG/DTA of NCO in air atmosphere b) XRD pattern of NCO at 800 °C c) ^{23}Na NMR spectra for NCO at different relaxation time intervals and d) FTIR transmittance spectra for NCO.

^{23}Na NMR spectra^{30,31} has been recorded for NCO at different relaxation times namely 1, 5, 25 s, (with respect to CH_3COONa as a reference) which is shown in Fig. 1c. From Fig.1c it is observed that it has two chemical shifts (CS), at 5.55 and -17.7 ppm corresponding to ^{23}Na . The results predicts that Na has occupied in two different trigonal prismatic sites in the parent crystal.²⁴ Positive CS value explains that (5.55 ppm) Na atom is surrounded by less number of neighbouring atoms, i.e., it shares the face with two CoO_6 octahedra (Na_f) of the lattice²⁴. On the other hand, negative CS value (-17.7 ppm) indicates that Na atom is surrounded by more number of neighbouring atoms (Na_e) by edge sharing with six CoO_6 octahedra.²⁴ Fig. 2, explains the FE-SEM images of synthesized NCO, sintered at 800 °C and morphology indicates that particles are uniformly distributed and having well defined hexagonal shape with particle size ranging from 1-3 μm . The small white spots are

present on the surface of the particle which may be a negligible amount of Na_2CO_3 phase¹⁹, Delmas et.al., explained that sodium is existing in two sites (Na_e , Na_f) in NCO ²⁴, wherein, Na_f are weakly bound. So, weakly bound sodium may reacts with atmospheric air and forms Na_2CO_3 as a minor impurity. Fig. S2 illustrates the images of the cycled electrode, where, the particle size is completely reduced and it is ranging ~ 200 nm. Furthermore, the small impurity present could not be identified by XRD analysis. Transmittance FTIR spectra for NCO has been recorded, which is shown in Fig.1d. The peak at 567 cm^{-1} , confirms the Co-O ³² bond formation, apart from this other peak at 1452 cm^{-1} , which confirms that the Na-O ³³ bond, in NCO.

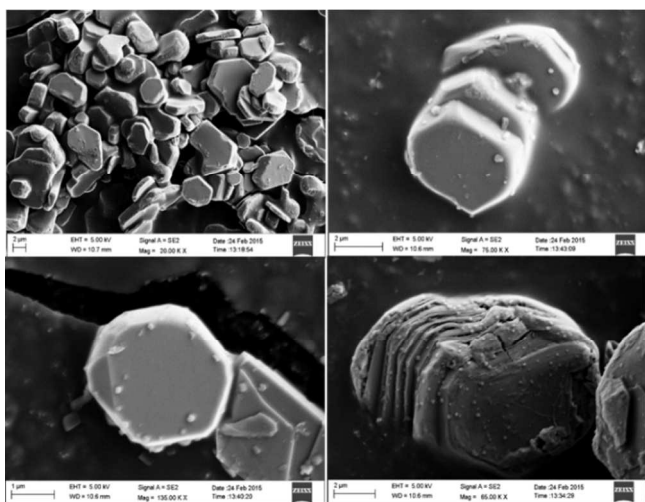


Fig.2 FE-SEM images of NCO at different magnifications.

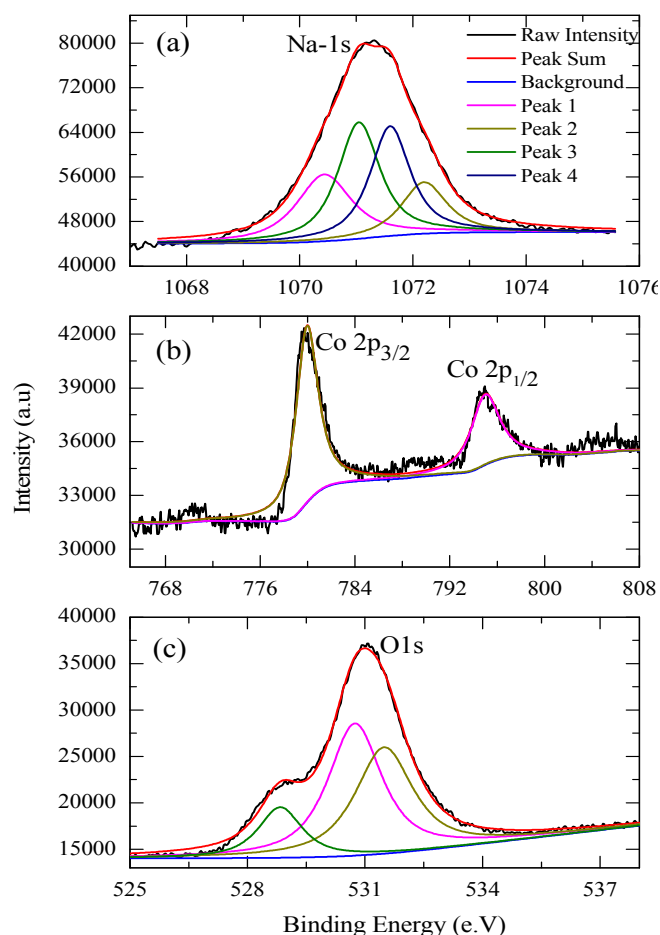


Fig.3 a) XPS spectra of Na b) XPS spectra of Co c) XPS spectra of O.

The binding energy (BE) value at 1071.4 eV which as show in Fig. 3a corresponds to $\text{Na } 1s$ and it is confirms that the Na^+ is bound with oxygen.³⁴ Cobalt is having two major BE values at 779.8 and 795 eV , which corresponds to $\text{Co}2p_{3/2}$, $\text{Co}2p_{1/2}$ spin states, the small variation binding energy values with respect to the chemical environment of Cobalt has been illustrated in the supporting information. which is confirmed by the observed BE values attributed to the Co-O interactions thereby indicating Cobalt is in $+3$ oxidation state and it is electrochemically active³² (Fig.3b). Fig.3c., shows that Oxygen $1s$ binding energy values at 529 eV and 531 eV , it is corresponding to the oxygen position at different environments (Na-O and Co-O) in NCO crystal structure.³²

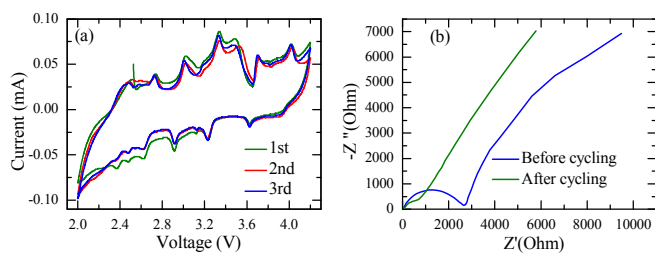


Fig.4 a) CV for NCO at scan rate of 0.1 mVs^{-1} b) EIS for NCO before and after cycling.

Fig. 4a. Explains the CV studies of NCO cycled between 2.0 - 4.2 V at a scan rate of 0.1 mV s⁻¹ (OCV is 2.5 V). The voltammogram illustrates several peaks (2.4, 2.5, 2.7, 3.0, 3.3, 3.4, 3.7, and 4.0 V) which are observed during anodic sweep and the corresponding cathodic peaks (3.9, 3.6, 3.2, 3.1, 2.9, 2.6, 2.4 and 2.3 V), which confirms the reversibility of Na⁺. Occurrence of several peaks in the CV profile at anodic as well as cathodic region are due to the formation of different intermediate chemical composition during the Na⁺ intercalation and de-intercalation.²⁴ Unlike, the conventional lithium-ion battery chemistry, the sodium-ion battery chemistry differs in Na⁺ intercalation/de-intercalation occurring at wider potential window. This complex behaviour in CV is generally observed in sodium metal oxide based materials.³⁵ In order to understand the interfacial reaction between electrode and electrolytes, the EIS has been recorded for Na-ion coin cell before and after cycling in the frequency range 100 kHz to 5 mHz (Fig. 4b). The Nyquist plots display that the charge transfer resistance drastically reduces for the cycled cell than the initial cell, which, indicates that the improvement of interfacial conductivity for the faster charge transfer between the electrode and electrolyte because of the efficient SEI formation at the surface of the electrode.^{36,37} Double layer capacitance (C_{dl}) of the NCO has been calculated for the same cell using the equation³⁸ (1) before and after cycling and the corresponding values have been tabulated (Table 1).

$$C_{dl} = \frac{1}{R_{ct}2\pi f_{max}} \quad \text{-----1}$$

Further, the diffusion coefficient of the Na (D_{Na⁺}) of the cell has been derived using the following formula.³⁹

$$D = \frac{R^2T^2}{2A^2n^4F^4C^2\sigma^2} \quad \text{----- 2}$$

Where, 'A' is the area of the electrode (cm²), n is the number of electrons transferred, 'F' (coulomb/mol) is the Faraday constant, 'C' is concentration (mol cm⁻³), σ is the coefficient of Warburg impedance, 'R' is the gas constant (J K⁻¹ mol⁻¹), T is the absolute temperature (K), σ is obtained from the extrapolation of straight line (low frequency region) from the semicircle to real axis and is equal to (R_s + R_{ct} - 2σ²C_{dl}).⁴⁰ The activation energy of the material has been calculated using following formula⁴¹.

$$D = D_0 e^{(-A/RT)} \quad \text{----- 3}$$

Where the 'A' is the activation energy (eV/atom), 'R' is the rate constant (eV/atom-K), 'D' is diffusion coefficients (cm²/sec), 'D₀' is the temperature-independent pre exponential (m²/s) and 'T' is the absolute temperature (K).

Table1. EIS parameters calculated from Nyquist plot before and after cycling for NCO.

S.No	Parameters	Before cycling	After cycling
1	R _s (Ω)	66.29	78.29
2	R _{ct} (Ω)	2664.91	422.32
3	C _{dl} (F)	0.598x10 ⁻⁹	3.771x10 ⁻⁹
4	D _{Na⁺} (cm ² /sec)	2.7x10 ⁻¹²	2.2x10 ⁻¹⁰
5	Activation energy(eV/atom)	~1.0	~0.7

The solution resistance is slightly increasing after 50 cycles, which may be attributed due to a passive layer formation at the interface due to decomposition of electrolytic solution, which, affects the sodium mobility at the interface.⁴² Consequently, this behaviour is also reflected in the charge/discharge profile as well and after prolonged cycling slight capacity fade is observed and correspondingly the activation energy NCO (before and after cycling) also decreases. Diffusion coefficient values show that the drastic increase (100 times) after 50 cycles.⁴³ These observed values well correlated with earlier reports. Before cycling the activation energy value is ~1 eV/atom and after cycling the activation energy value is ~0.7eV/atom indicating the activity of the Na⁺ increases upon cycling⁴⁴. Galvanostatic charge/discharge performance of NCO have been tested at different C-rates (0.1, 0.2, 0.5 and 1 C) as shown in Fig. 5a for determining the rate tolerance of the material. At 0.1, 0.2, 0.5 and 1C rates, first cycle discharge capacities are 126, 108, 77 and 43 mAh g⁻¹ respectively. At 0.1 C rate tenth cycle discharge capacity is 113 mAhg⁻¹ with ~90 % capacity retention. Initially, at 0.1 C the specific capacity decreases and attains a steady state after sixth cycle and can be attributed due to the formation of SEI layer. In order to investigate the rate capability of the material, same cell have been continued for cycling at 0.2 C, 0.5 and 1 C rates. At 0.5 C rate the cell delivers the discharge capacity of ~ 70 mAh g⁻¹ with 95 % capacity retention. Rate capability studies were done after 50 cycles at 0.1C and C rate, as shown in Fig 5a. Fig. 5b. depicts that the charge/discharge profile of NCO at different C-rates. At high C rate, plateaus are disappeared (supported with CV data (Fig. S3)) which may be due to the high activation polarization, developed, when applying high current between the electrodes. At 0.1 C rate anodic and cathodic plateaus are clearly visible at 4.1, 3.7, 3.3, 2.9, 2.7 and 3.8, 3.5, 3.2, 2.8, 2.6 V respectively. These plateaus are quite consistent with the redox couples observed in cyclic voltammetry studies at 0.1 mV s⁻¹.

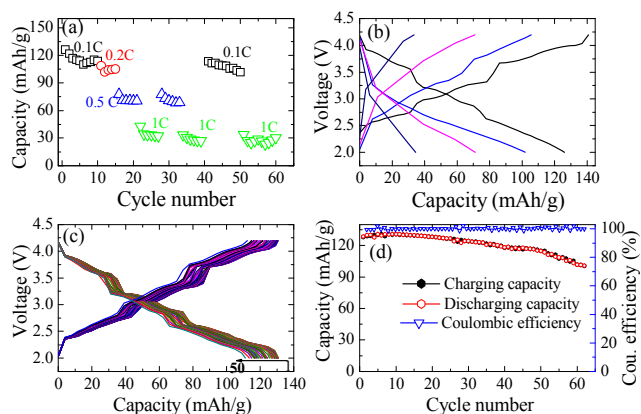


Fig. 5. a) Rate capability of NCO b) Charge/discharge profile of NCO at different C rates c) Charge discharge profile of NCO at 0.1 C rate and d) Life cycle performance of NCO at 0.1 C rate.

At 0.1 C rate, charge/discharge profile of NCO is shown in Fig. 5c up to 50 cycles, which shows that steps like behaviour, suggesting that different chemical composition formed during cycling, which is also supported by earlier reports.^{24–26} Fig. 5d shows the capacity obtained after prolonged cycling (50 cycles) delivering an average discharge capacity of 121 mAhg⁻¹ with 99.99 % coulombic efficiency which is quite interesting in the present work. Charge /discharge capacities of 1, 10, 20, 30, 40 and 50 cycles are 127/128, 130/130, 128/128, 124/124 and 118/118 mAh g⁻¹ respectively. At 0.1 C rate the discharge capacities reported here in are better than earlier reports.

Conclusions

In the present work, NCO has been presented as a cathode material for sodium rechargeable batteries, which is synthesized by sol-gel technique using glycine as a chelating as well as fuel. FESEM shows that particles are present in the range of 1–3 μm. At 0.1 C rate after prolonged cycling (50 cycles), it delivers average discharging capacity of 121 mAh g⁻¹ with 99.99 % coulombic efficiency.

Acknowledgements

One of the authors B. Venkata Rami Reddy wishes thanks to UGC, India for senior research fellowship.

Notes and references

*^aCorresponding author

CSIR–Central Electrochemical Research Institute (CSIR–CECRI), Karaikudi, 630006, India.
E-mail: gopukumar@cecri.res.in
Fax: +914565227779

^b Department of Energy and Environment, National Institute of Technology, Tiruchirappalli.

References

- 1 I. Belharouak, *LITHIUM ION BATTERIES– NEW DEVELOPMENTS*, 2012.
- 2 D. Linden and T. B. Reddy, *Handbook of Batteries*, 2001.
- 3 V. Palomares, M. Casas-Cabanas, E. Castillo-Martinez, M. H. Han and T. Rojo, *Energy Environ. Sci.*, 2013, **6**, 2312–2337.
- 4 S. W. Kim, D. H. Seo, X. Ma, G. Ceder and K. Kang, *Adv. Energy Mater.*, 2012, **2**, 710–721.
- 5 C. Nithya and S. Gopukumar, *Wiley Interdiscip. Rev. Energy Environ.*, 2015, **4**, 253–278.
- 6 N. Yabuuchi, K. Kubota, M. Dahbi and S. Komaba, *Chemical Rev.*, 2014, **114**, 11636–11682.
- 7 K. T. Lee, T. N. Ramesh, F. Nan, G. Botton and L. F. Nazar, *Chem. Mater.*, 2011, **23**, 3593–3600.
- 8 P. Barpanda, G. Liu, C. D. Ling, M. Tamaru, M. Avdeev, S. C. Chung, Y. Yamada and A. Yamada, *Chem. Mater.*, 2013, **25**, 3480–3487.
- 9 C. S. Park, H. Kim, R. a. Shakoob, E. Yang, S. Y. Lim, R. Kahraman, Y. Jung and J. W. Choi, *J. Am. Chem. Soc.*, 2013, **135**, 2787–2792.
- 10 A. Kitajou, H. Komatsu, K. Chihara, I. D. Gocheva, S. Okada and J. I. Yamaki, *J. Power Sources*, 2012, **198**, 389–392.
- 11 N. Dimov, A. Nishimura, K. Chihara, A. Kitajou, I. D. Gocheva and S. Okada, *Electrochim. Acta*, 2013, **110**, 214–220.
- 12 Z. Jian, L. Zhao, H. Pan, Y. S. Hu, H. Li, W. Chen and L. Chen, *Electrochem. commun.*, 2012, **14**, 86–89.
- 13 K. Saravanan, C. W. Mason, A. Rudola, K. H. Wong and P. Balaya, *Adv. Energy Mater.*, 2013, **3**, 444–450.
- 14 Q. L. Wang, a Madsen, J. R. Owen and M. T. Weller, *Chem. Commun.*, 2013, **49**, 2121–2123.
- 15 Y. Lu, S. Zhang, Y. Li, L. Xue, G. Xu and X. Zhang, *J. Power Sources*, 2014, **247**, 770–777.
- 16 Y. Lu, L. Wang, J. Cheng and J. B. Goodenough, *Chem. Commun.*, 2012, **48**, 6544–6546.
- 17 X. Ma, H. Chen and G. Ceder, *J. Electrochem. Soc.*, 2011, **158**, A1307–A1312.
- 18 P. Vassilaras, X. Ma, X. L. And and G. Ceder, *J. Electrochem. Soc.*, 2013, **160**, A207–A211.
- 19 M. Sathiya, K. Hemalatha, K. Ramesha, J.-M. Tarascon and a. S. Prakash, *Chem. Mater.*, 2012, **24**, 1846–1853.

ARTICLE

- 20 N. Yabuuchi, M. Kajiyama, J. Iwatate, H. Nishikawa, S. Hitomi, R. Okuyama, R. Usui, Y. Yamada and S. Komaba, *Nat. Mater.*, 2012, **11**, 512–517.
- 21 D. Buchholz, A. Moretti, R. Kloepsch, S. Nowak, V. Siozios, M. Winter and S. Passerini, *Chem. Mater.*, 2013, **25**, 142–148.
- 22 L.W.Shacklette, T. R. Jow and L.Townsend, *J. Electrochem. Soc.*, 1988, **135**, 2669–2674.
- 23 Y. Ma, M. M. Doeff, S. J. Visco and L. C. De Jonghe, *J. Electrochem. Soc.*, 1993, **140**, 2726–2733.
- 24 R. Berthelot, D. Carlier and C. Delmas, *Nat. Mater.*, 2011, **10**, 74–80.
- 25 M. D'Arienzo, R. Ruffo, R. Scotti, F. Morazzoni, C. M. Mari and S. Polizzi, *Phys. Chem. Chem. Phys.*, 2012, **14**, 5945–5952.
- 26 J. J. Ding, Y. N. Zhou, Q. Sun, X. Q. Yu, X. Q. Yang and Z. W. Fu, *Electrochim. Acta*, 2013, **87**, 388–393.
- 27 S. C. Han, H. Lim, J. Jeong, D. Ahn, W. B. Park, K.-S. Sohn and M. Pyo, *J. Power Sources*, 2015, **277**, 9–16.
- 28 B. Venkata Rami Reddy and S. Gopukumar, *ECS Trans.*, 2013, **53**, 49–58.
- 29 A. Sivashanmugam, R. Thirunakaran, M. Zou, M. Yoshio, J. Yamaki and S. Gopukumar, *J. Electrochem. Soc.*, 2006, **153**, A497–A503.
- 30 C. P. Grey and N. Dupré, *Chem. Rev.*, 2004, **104**, 4493–4512.
- 31 D. Carlier, M. Blangero, M. Ménétrier, M. Pollet, J. P. Doumerc and C. Delmas, *Inorg. Chem.*, 2009, **48**, 7018–7025.
- 32 C. Nithya, R. Thirunakaran, a. Sivashanmugam and S. Gopukumar, *J. Power Sources*, 2011, **196**, 6788–6793.
- 33 M. Shirpour, J. Cabana and M. Doeff, *Energy Environ. Sci.*, 2013, **6**, 2538–2547.
- 34 C. D. Wagner, W. M. Riggs, L. E. Davis and J. F. Moulder, *Handbook of X-ray Photoelectron Spectroscopy*, 1979.
- 35 Y. Cao, L. Xiao, W. Wang, D. Choi, Z. Nie, J. Yu, L. V. Saraf, Z. Yang and J. Liu, *Adv. Mater.*, 2011, **23**, 3155–3160.
- 36 C. Nithya and S. Gopukumar, *J. Mater. Chem. A*, 2014, **2**, 10516–10525.
- 37 R. Ravikumar and S. Gopukumar, *Phys. Chem. Chem. Phys.*, 2013, **15**, 3712–3717.
- 38 A. J. Bard and L. R. Faulkner, *Electrochemical methods : fundamentals and applications*, 2001.
- 39 B. Jin, E. M. Jin, K.-H. Park and H.-B. Gu, *Electrochem. commun.*, 2008, **10**, 1537–1540.
- 40 M. Shi, Z. Chen and J. Sun, *Cem. Concr. Res.*, 1999, **29**, 1111–1115.
- 41 W. D. Callister and D. G. Rethwisch, *Fundamentals of materials science and engineering: an integrated approach*, John Wiley & Sons, 2012.
- 42 S. T. Myung, K. Izumi, S. Komaba, Y. K. Sun, H. Yashiro and N. Kumagai, *Chem. Mater.*, 2005, **17**, 3695–3704.
- 43 S. Kikkawa, S. Miyazaki and M. Koizumi, *J. Power Sources*, 1985, **14**, 231–234.
- 44 M. Okubo, Y. Tanaka, H. Zhou, T. Kudo and I. Honma, *J. Phys. Chem. B*, 2009, **113**, 2840–2847.